![Lund University seal]

LUND UNIVERSITY

Laser-accelerated protons with energy dependent beam direction

Lindau, Filip; Lundh, Olle; Persson, Anders; McKenna, Paul; Osvay, K; Batani, D; Wahlström, Claes-Göran

Link to publication

P H Y S I C A L   R E V I E W   L E T T E R S

Laser-Accelerated Protons with Energy-Dependent Beam Direction

F. Lindau,[1] O. Lundh,[1] A. Persson,[1] P. McKenna,[2] K. Osvay,[1,*] D. Batani,[3,†] and C.-G. Wahlström[1]

[1]*Department of Physics, Lund Institute of Technology, P.O. Box 118, S-22100 Lund, Sweden*
[2]*Department of Physics, University of Strathclyde, Glasgow G4 0NG, United Kingdom*
[3]*Dipartimento di Fisica "G. Occhialini," Università di Milano Bicocca, Piazza della Scienza 3, 20126 Milano, Italy*

The spatial distribution of protons, accelerated by intense femtosecond laser pulses interacting with thin target foils under oblique irradiation are investigated. Under certain conditions, the proton beams are directed away from the target normal. This deviation is towards the laser forward direction, with an angle that increases with the level and duration of the amplified spontaneous emission pedestal before the main laser pulse. In addition, for a given laser pulse, this beam deviation increases with proton energy. The observations are discussed in terms of different electron acceleration mechanisms and target normal sheath acceleration, in combination with a laser-controllable shock wave locally deforming the target rear surface.

The generation of intense beams of energetic protons using short-pulse high-intensity lasers has recently attracted great interest. One of the most characteristic features of short-pulse laser acceleration of protons from thin solid targets is the directed beams emerging from the back of the target, in the target normal direction, and with a divergence decreasing with increasing proton energy [1]. With the laser focused obliquely onto the target, Krushelnick *et al.* [2] found that under certain conditions two separate spatial distributions could be observed in the proton emission. Deviation from target normal was observed also by Zepf *et al.* [3] on some of the laser shots in their investigations.

We present in this Letter a study on the spatial distribution of laser-accelerated protons. In particular, we study systematically the direction of the proton beam, as a function of various target and laser parameters, with the laser focused obliquely onto the target foil. We find that the proton beams are not always directed along the target normal, but under certain conditions steered towards the laser forward direction. We also show, for the first time, that the angle of deviation depends on the proton energy, and that it can be optically controlled by varying the intensity and duration of the ASE (amplified spontaneous emission) pedestal.

The experiments are performed with the 10 Hz multi-terawatt femtosecond laser at the Lund Laser Centre. It is a Ti:sapphire system delivering 35 fs pulses of up to 35 TW at 800 nm. Important features of this system are that it allows the level and duration of the ASE pedestal, as well as the final pulse energy, to be continuously varied. The ratio between the peak and pedestal intensities, being the temporal contrast, is measured in the flat part of the pedestal before the main pulse, using a third order autocorrelator. (The ASE intensity is estimated from the measured contrast value and the estimated peak intensity.) Fast Pockels cells are incorporated in the system to enable

efficient suppression of any prepulses and to facilitate control of the duration of the ASE pedestal—in the range 1.0–4.5 ns.

An $f/3$, off-axis parabolic mirror is used to focus the laser beam to a $\sim 10\ \mu$m diameter spot ($1/e^2$). From the spot size, pulse duration, and pulse energy (700 mJ on target), we infer a peak intensity exceeding 10^{19} W/cm^2. At the focus, target foils of different materials and thicknesses are mounted for p-polarized irradiation at 45° angle of incidence.

The spatial distribution of the laser-accelerated protons is diagnosed with CR-39 nuclear track detectors, sensitive to protons but insensitive to electrons and x rays [4], placed 25 mm behind the target and oriented parallel to the target foil. A filter mask is positioned directly in front of the detector plates. This enables measurement of the spatial distributions of protons above chosen threshold energies; see Fig. 1(a).

With this setup we detect a broad energy distribution of protons, extending beyond 4 MeV, in a beam which is always in the plane of the laser beam and the target normal. Most unexpectedly, we find that under certain target and laser conditions, the proton beams are directed away from the target normal, towards the laser direction, by an angle that increases with proton energy. This is illustrated in Fig. 1(d) by a typical example obtained with 6 μm Al target.

In order to investigate these observations further, we perform a series of experiments where we systematically vary the target thickness, pedestal duration, and contrast ratio (pedestal intensity). The results are illustrated in Fig. 2, where data from typical, representative CR-39 detector plates, recorded during the same experimental runs are compared. These show that the observed energy-dependent beam deviation, away from target normal, can be optically controlled by carefully selecting the level and duration of the ASE pedestal. For a 6 μm Al target and a
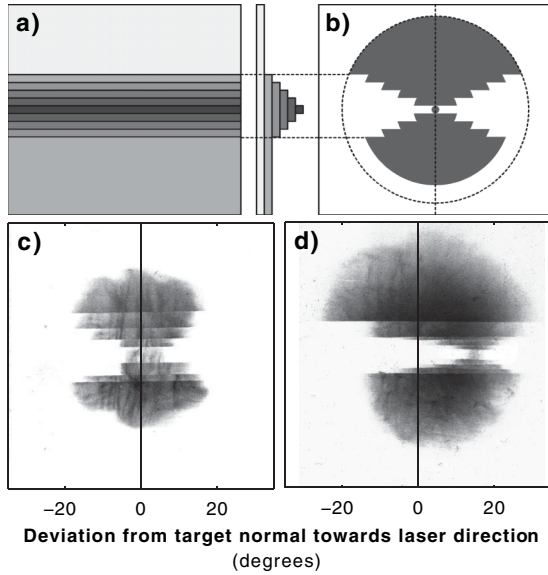
FIG. 1.   (a) An Al filter mask is placed in front of the CR-39 plates to enable measurement of both the proton spatial and energy distributions. The expected pattern on the detector plates is schematically illustrated in (b), assuming a proton beam directed along the target normal and with a divergence decreasing with increasing proton energy. The observed distributions are illustrated by two representative examples obtained with (c) 12 μm and (d) 6 μm Al target. These examples clearly show that the proton beam under some conditions is centered along the target normal, and under other conditions shifted away, towards the laser direction, with an angle of deviation increasing with proton energy. The filter thickness used in the two cases are different, corresponding to a maximum threshold energy of 2.5 and 4.8 MeV in (c) and (d), respectively.

sufficiently low ASE level, proton beam steering requires the ASE pedestal to be extended in time beyond its minimum value. Alternatively, with a minimum pedestal duration (1 ns), the ASE level must be increased beyond its minimum value ($\sim 1 \times 10^{12}$ W/cm^2). In addition to the systematic trends observed regarding beam directions, we find that the smallest beam divergence is obtained with the shortest pedestal and the best contrast. This is illustrated by the cases shown in Figs. 2(b) and 2(c), where the divergence increases with ASE duration and level, respectively. The dependency on target thickness, illustrated in Fig. 2(a), indicates that the observed beam steering cannot be due to processes occurring on the target front surface only. In addition, not shown in Fig. 2 are our findings that energy-dependent beam deviations are observed also with 12 μm targets if the pedestal duration, or intensity, is increased sufficiently beyond its minimum value, and that with a too high ASE level no protons with energy above 1.6 MeV are observed with 6 μm targets.

The observed beam deviation from target normal might at first appear to be in conflict with the target normal sheath acceleration, TNSA, mechanism [5], by which the proton beams are emitted normal to the target rear surface. However, as discussed by Wilks *et al.* [5] and demonstrated
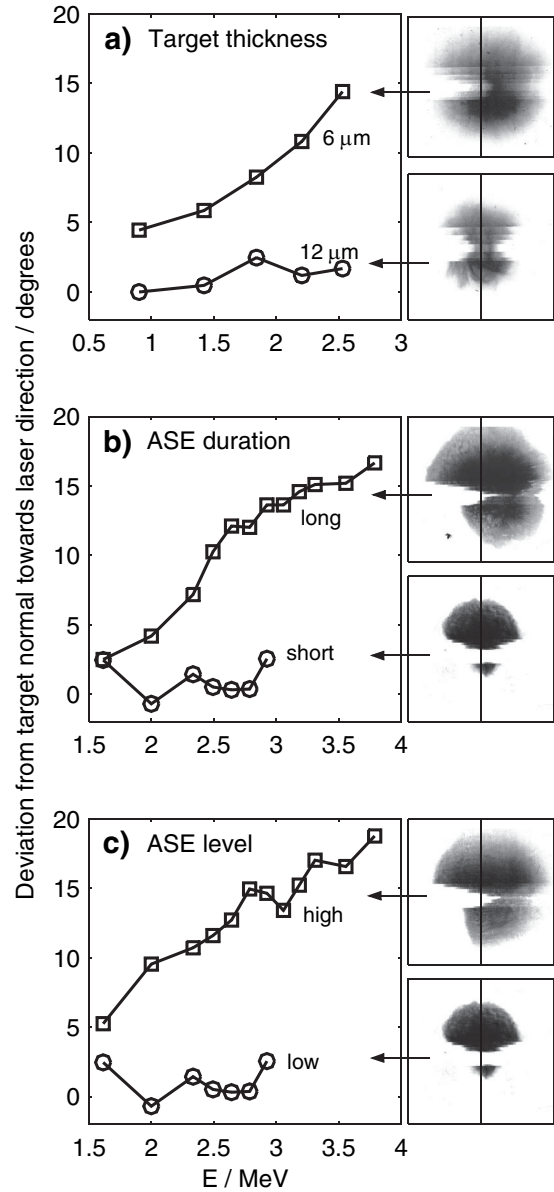

FIG. 2.   Deviation from target normal for protons above different threshold energies. The lines through the images on the right indicate target normal direction. With the pedestal duration increased by 1 ns from its minimum value and a contrast of 3×10^7, the target thickness is varied in (a) from 12 to 6 μm. With 6 μm target thickness and a setting with minimum pedestal duration (~ 1 ns) and a contrast of 3×10^7, (b) illustrates the effect of increasing the pedestal duration by 1 ns and (c) of decreasing the contrast (increasing the ASE level) to 6×10^6, corresponding to an estimated ASE intensity of 5×10^{12} W/cm^2.

by Roth *et al.* [6], this mechanism facilitates proton beam manipulation (focusing and defocusing) by using targets with curved rear surfaces. With this in mind, we propose the following explanation for the observed beam deflection: a shock wave is launched into the target, along the target normal, by the ablation pressure induced on the front surface by the ASE pedestal. When this shock wave

reaches the back side it gives rise to a dynamic expansion of the rear surface, which thus becomes convex with a time-dependent curvature. In experiments performed with the laser at normal incidence, this would, at most, result in an increased beam divergence.

To understand the beam deflection observed in our experiments, performed at 45° angle of incidence, we need to consider also the direction of the electrons heated by the laser at the target front surface. Different acceleration mechanisms exist and have different relative importance at different laser intensities and preplasma conditions. At "low" intensities, or steep plasma density gradients, resonant absorption dominates, accelerating electrons predominately along the target normal. At higher (relativistic) intensities and sufficiently large preplasmas, electrons are accelerated also in the laser forward direction by the $\mathbf{v} \times \mathbf{B}$ force of the intense laser radiation. This leads to the generation of two distinct electron distributions, along the target normal and in the forward laser propagation direction. This was first studied by Santala *et al.* [7], exploring the relative importance of the plasma density scale length on the two electron distributions. Later, Brandl *et al.* [8] showed that at high intensities, the highest electron energies are in the forward directed distribution. In our study the size of the preplasma varies with the ASE conditions. Simulations using the code MULTI, discussed below, show that the size, as determined by the distance from the ablation front to the critical density, ranges from a few μm at the lowest ASE levels and shortest durations, to 10–20 μm for the higher ASE intensities. Under the ASE conditions leading to the observed energy-dependent proton direction, the preplasma thus supports both heating mechanisms. However, we emphasize that the varying preplasma conditions alone cannot explain the experimental observations, in particular, not the dependence on target thickness of the ASE controlled proton beam deviation.

The electron distributions produced by the two different mechanisms both have certain angular spreads, so at the rear surface they can partly overlap. However, the center positions are different. If the rear surface has had time to expand, and become convex before the arrival of the main pulse, the central part of the two electron distributions will therefore leave the surface where the "local target normal" is pointing in different directions. In particular, the most energetic, forward accelerated electrons will leave the target surface where the local target normal is steered towards the laser forward direction (see inset of Fig. 3). The most energetic protons will consequently be accelerated, by TNSA, in this direction, while the low-energy proton distribution will mainly be defocused by the convex target surface. The curvature of the rear surface, and the partly overlapping electron distributions, result in a continuous spread of proton directions and not two separate beams.

The breakout of a shock wave at the rear target surface is frequently assumed to ruin the steep density gradient and thus prohibit efficient rear surface ion acceleration. A key
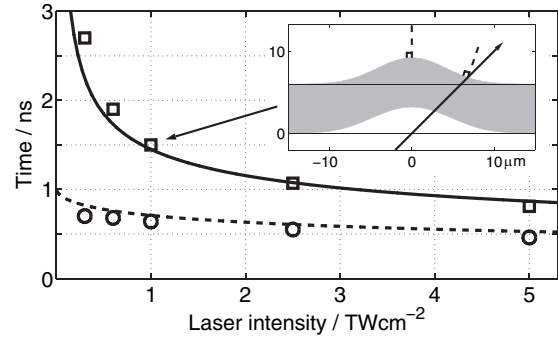

FIG. 3.   The time required for a laser-driven shock to pass through a 6 μm Al target is plotted as a function of the laser (ASE) intensity (dashed line), as well as the total time for the shock to pass through the target and for the rear surface to expand 3 μm into vacuum (solid line). The analytical results are compared with results of 1D-hydrodynamic simulations giving the shock breakout time (circles) and the expansion time up to 3 μm (squares). The inset illustrates the results from 2D-hydrodynamic simulations, showing the ablation front at the front target surface and the expansion of the rear surface before the arrival of the main pulse. The arrow points in the direction of the laser propagation axis. The intensity and duration of the ASE pedestal match the indicated data point in the main figure.

point in the proposed explanation of our observations is therefore the assumption that, within our range of target and laser-pedestal parameters, an ASE-driven shock wave can give rise to a deformation of the target rear surface without melting it. In aluminum, the shock pressure P required to reach melting along the Hugoniot is approximately 1.2 Mbar ($=120$ GPa) [9]. This pressure corresponds to a melting temperature along the Hugoniot of about 5200 K (0.45 eV), much higher than even the boiling temperature for Al in standard conditions (2792 K). Such a change of regime in shock dynamics was recently studied experimentally using optical diagnostics [10].

The shock wave is driven by laser ablation on the front surface. Ablation pressure scales with laser intensity approximately as $I^{2/3}$ and, for Al and our laser wavelength, a pressure of 1.2 Mbar is reached at $\approx 4.2 \times 10^{12}$ W/cm^2 [11,12]. In our experiments we vary, and measure, the ASE contrast over more than 1 order of magnitude, with 3×10^7 being the highest value. With the peak laser intensity estimated to 3×10^{19} W/cm^2, this gives a variable pedestal intensity ranging from 1×10^{12} W/cm^2 to several times 10^{13} W/cm^2. This range of ASE intensities thus allows shock waves with shock temperatures below as well as above the melting point of the compressed target material to be studied.

Next we estimate the time required for the shock to pass through the target and to develop a rear surface curvature. At very low pressures, the shock velocity u_s is close to the bulk sound velocity c_0 but increases with shock pressure. The shock velocity is related to the particle velocity u_p as $u_s = c_0 + \alpha \times u_p$ ($\alpha = 1.21$, and $c_0 = 6.0$ μm/ns in Al [9]). The particle velocity and the shock wave velocity are

related through the momentum conservation relation $\rho_0 u_s u_p = P$, where ρ_0 is the initial target density and P the shock pressure. When the shock wave reaches the rear surface of the solid target, the free surface starts moving into vacuum with a velocity $u_{FS} \approx 2u_p$ while a rarefaction wave is backscattered into the medium [13]. In Fig. 3 we plot, as functions of laser intensity, the time it takes for a shock wave to pass through a 6 μm thick target and for the rear surface, with velocity u_{FS}, to move 3 μm, as an example of deformation giving a significant target curvature. (We assume a temporally flattop intensity profile for the ASE pedestal.) The analytic results are verified by hydrodynamic simulations performed with the code MULTI [14] and equation-of-state data for Al from [9]. We find good agreement between the analytical results and the hydrodynamic simulation. In addition, the MULTI simulations confirm that at these intensities, the density profile at the rear surface remains a step function during the expansion. From this figure we find that, with the ASE intensity corresponding to our best contrast, $\sim 1 \times 10^{12}$ W/cm^2, and our minimum ASE duration, 1 ns, there will not be time to produce the given rear surface deformation before the arrival of the main pulse. But by increasing either the ASE duration by 1 ns or the shock pressure (ASE intensity) to the maximum pressure without melting, 1.2 Mbar (4.2×10^{12} W/cm^2), the rear surface will have time to deform before the arrival of the main pulse. These estimates also show that an increase in target thickness requires an increase in pedestal duration, or in ASE intensity, for the same beam deviation to be observed as with thinner targets. These dependencies, with respect to ASE intensity, pedestal duration, and target thickness all agree qualitatively with the trends observed experimentally and illustrated in Fig. 2.

In order to verify that the rear surface deformation is consistent with the observed proton deflection, we perform two-dimensional hydrodynamic simulations using the code MULTI-2D [15] with parameters chosen to mimic the experimental conditions (flattop laser intensity profile with 14 μm $1/e^2$ diameter Gaussian spot, target simulated with data from the Sesame tables). One example of the results is shown in the inset of Fig. 3. The limits of the gray regions correspond to the position of the surface where the mass density equals the initial mass density in the solid, unperturbed, target. The "local target normal," where the laser axis exits the rear surface, deviates from the global target normal, towards the laser forward direction, in agreement with the observed proton beam deflections. More detailed comparisons between experimental results and modeling will be published separately.

The findings reported in this Letter have immediate implication in a variety of situations. First, they directly influence the proper design of experimental studies. For example, Thomson parabola ion spectrometers are frequently employed to diagnose the accelerated ions.

Whereas this technique supports measurement of the continuous energy distribution of the ions, it is limited to sampling a small solid angle. The results of the present study clearly show that the positioning of the ion spectrometer can influence the recorded energy distribution. Second, the present result addresses the fundamental processes involved in the transfer of laser energy to energetic protons, via energetic and directed electrons. Further studies of these energy-dependent beam directions should allow the different processes involved to be further disentangled and understood, which is of utmost importance for efficient optimization of the beam properties. Finally, they open new perspective for novel applications, where active control of the divergence, direction, and spatial energy distribution of beams of laser-accelerated ions are essential. It is conceivable, for example, that the observed phenomenon could be used to tailor the beams such that ions of selected energy are preferentially deflected or focused in specific directions.

*Present address: Department of Optics and Quantum Electronics, University of Szeged, Szeged 6701, Hungary.
†On leave at LOA, Ecole Polytechnique, Palaiseau, France.
[1] R. A. Snavely *et al.*, Phys. Rev. Lett. **85**, 2945 (2000).
[2] K. Krushelnick *et al.*, Phys. Plasmas **7**, 2055 (2000).
[3] M. Zepf *et al.*, Phys. Plasmas **8**, 2323 (2001).
[4] F. H. Seguin *et al.*, Rev. Sci. Instrum. **74**, 975 (2003).
[5] S. C. Wilks *et al.*, Phys. Plasmas **8**, 542 (2001).
[6] M. Roth *et al.*, Plasma Phys. Controlled Fusion **44**, B99 (2002).
[7] M. I. K. Santala *et al.*, Phys. Rev. Lett. **84**, 1459 (2000).
[8] F. Brandl *et al.*, Europhys. Lett. **61**, 632 (2003).
[9] Sesame tables 3712 and 3717 for Al, from T4 Group LANL, SESAME Report on the Los Alamos Equation-of-State Library, Report No. LALP-83-4, 1983.
[10] A. Benuzzi-Mounaix *et al.*, Phys. Rev. E **70**, 045401 (2004).
[11] D. C. Swift *et al.*, Phys. Rev. E **69**, 036406 (2004).
[12] J. Lindl, Phys. Plasmas **2**, 3933 (1995).
[13] Ya. B. Zeldovich and Yu. P. Raizer, *Physics of Shock Waves and High Temperature Hydrodynamic Phenomena* (Academic Press, New York, 1967).
[14] R. Ramis, R. Schmalz, and J. Meyer-ter-Vehn, Comput. Phys. Commun. **49**, 475 (1988).
[15] R. Ramis and J. Meyer-ter-Vehn, Max-Planck-Institut für Quantenoptik, Report No. MPQ174, 1992.